Applied Numerical Mathematics 62 (2012) 185–200

Contents lists available at SciVerse ScienceDirect

Applied Numerical Mathematics

www.elsevier.com/locate/apnum

Homotopy method for a mean curvature-based denoising model ☆

Fenlin Yang [a,c], Ke Chen [b,*], Bo Yu [a]

[a] School of Mathematical Sciences, Dalian University of Technology, Dalian, Liaoning 116024, PR China
[b] Centre for Mathematical Imaging Techniques and Department of Mathematical Sciences, The University of Liverpool, Liverpool L69 7ZL, United Kingdom
[c] Department of Mathematics, Jishou University, Jishou, Hunan 416000, PR China

ARTICLE INFO

Article history:
Received 3 November 2010
Received in revised form 23 November 2011
Accepted 3 December 2011
Available online 7 December 2011

Keywords:
Image denoising
Total variation
Mean curvature
Fixed point curvature method
Homotopy method

ABSTRACT

Variational image denoising models based on regularization of gradients have been extensively studied. The total variation model by Rudin, Osher, and Fatemi (1992) [38] can preserve edges well but for images without edges (jumps), the solution to this model has the undesirable staircasing effect. To overcome this, mean curvature-based energy minimization models offer one approach for restoring both smooth (no edges) and nonsmooth (with edges) images. As such models lead to fourth order (instead of the usual second order) nonlinear partial differential equations, development of fast solvers is a challenging task. Previously stabilized fixed point methods and their associated multigrid methods were developed but the underlying operators must be regularized by a relatively large parameter. In this paper, we first present a fixed point curvature method for solving such equations and then propose a homotopy approach for varying the regularized parameter so that the Newton type method becomes applicable in a predictor–corrector framework. Numerical experiments show that both of our methods are able to maintain all important information in the image, and at the same time to filter out noise.

1. Introduction

An observed image can be contaminated with noise during recording and transmission. The common additive degradation model is

$$f = u + \eta. \tag{1}$$

Here f is the observed image (known), u is the desired true image (unknown), and η is an additive noise term (also unknown); these three quantities are functions defined on a bounded convex region Ω of $\mathbb{R}^d$ ($d = 2$ or 3, in this paper, the 2-dimensional case is considered and we will assume Ω is a square in $\mathbb{R}^2$). For other noise types, refer to [26,12]. The task of image denoising is to remove noise while preserving the main features such as edges of the original image, which is a phase before doing further image processing tasks e.g. edge detection, segmentation, pattern recognition, and object tracking.

The traditional modeling methods to estimate u based on least squares [41], although simple to implement, lead to results likely to be contaminated by Gibbs' phenomena (ringing) near edges. The total variation (TV) model proposed by

☆ The research was supported by the National Natural Science Foundation of China (10671029) and the Research Fund for the Doctoral Programme of Higher Education (20060141029).

* Corresponding author.
E-mail address: k.chen@liverpool.ac.uk (K. Chen).
URL: http://www.liv.ac.uk/www/cmit (K. Chen).

0168-9274/$36.00 © 2011 IMACS. Published by Elsevier B.V. All rights reserved.
doi:10.1016/j.apnum.2011.12.001

Rudin, Osher, and Fatemi (ROF) [38] can produce desirable results from removing noise while preserving edges for non-smooth images. But for smooth images, the ROF model suffers from staircasing effect, namely, the transformation of smooth regions (ramps) into piecewise constant regions (stairs). Therefore, the model cannot preserve finer details, such as texture and round shapes. Besides this effect, it cannot preserve the intensity contrasts. In recent years, among others, researchers have turned to higher order models [6,7,11,14,15,5,29,17,46] to remedy these unfavorable properties for a satisfactory result; see also [8,21,22,25,39,30,28,32,36].

One effective model aiming to improve the ROF [38] is the mean curvature-based energy minimization model by Zhu and Chan [46] where the new geometric quantity – the mean curvature of the induced image surface – is introduced and a piecewise smooth surface $(x, y, u(x, y))$ is used to approximate the image surface $(x, y, f(x, y))$. However, the resulting fourth order partial differential equations (PDE) arising from minimization of this model is nontrivial to solve due to appearance of a high nonlinearity and stiffness term, because simple alternative methods (which worked for the TV model) such as lagged fixed point methods [41,42] and primal–dual methods [13] do not work for this newer model, as shown in [6]. Another possible alternative for solving the mean curvature model is the split method [44,23] where one approximates the original functional by a new functional, leading to a system of second order PDEs by introducing an intermediate variable. In this paper, we propose a fixed point curvature method to solve a fourth order PDE using a homotopy technique to achieve fast convergence.

Other recent and effective models, that are not studied in this paper, for improving the ROF model [38] include the total generalized variation (TGV) method [5] and the nonlocal means based total variation (NLTV) based regularization method [8,21,25,28].

The rest of this paper is organized as follows. In Section 2, we introduce the mean curvature-based model and then review the existent numerical methods to solve this model. In Section 3, we present a fixed point curvature method for the curvature Euler–Lagrange equation, and in Section 4, we give a homotopy method using this fixed point curvature method as its correction. Finally, in Section 5, we present various numerical results obtained from the implementation of proposed algorithm.

2. Two algorithms for a mean curvature-based denoising model

For the sake of understanding the geometrical attributes which correspond to the signal information of corners, edges and intensity contrasts of an image, Zhu and Chan [46] introduced the mean curvature into an image denoising model with their energy functional represented as

$$\min_u \left\{ J(u) = \alpha \int_\Omega \Phi\big(\kappa(u)\big)\,dx\,dy + \frac{1}{2}\|u - f\|^2 \right\}, \tag{2}$$

where $f(x, y) \in L^2(\Omega)$ is the observed image, $u(x, y) \in C^2(\Omega)$ is the desired true image, $|\cdot|$ is the Euclidean norm in $\mathbb{R}^2$, and $\|\cdot\|$ is the norm in $L^2(\Omega)$. The functional Φ is defined either as $\Phi(\kappa(u)) = |\kappa(u)|$, $\Phi(\kappa(u)) = \kappa(u)^2$ or a combination of both, here $\kappa(u)$ is the mean curvature of the image which is defined by

$$\kappa(u) = \nabla \cdot \frac{\nabla u}{|\nabla u|}. \tag{3}$$

To avoid division by zero, we regularize the term $|\nabla u|$ by β, and define $|\nabla u|_\beta = \sqrt{|\nabla u|^2 + \beta}$. Thus, we have

$$\kappa_\beta(u) = \nabla \cdot \frac{\nabla u}{|\nabla u|_\beta}, \tag{4}$$

where β is a small positive parameter (see [41,42,34,31]), and the energy functional (2) becomes

$$\min_u \left\{ J_\beta(u) = \alpha \int_\Omega \Phi\big(\kappa_\beta(u)\big)\,dx\,dy + \frac{1}{2}\|u - f\|^2 \right\}. \tag{5}$$

The corresponding Euler–Lagrange partial differential equation (PDE) for (5) is, for $(x, y) \in \Omega$,

$$g_\beta(u) = \alpha \nabla \cdot \left(\frac{1}{|\nabla u|_\beta} \left(I_2 - \frac{\nabla u \nabla u^T}{|\nabla u|_\beta^2} \right) \nabla \Phi'\big(\kappa_\beta(u)\big) \right) + (u - f) = 0, \tag{6}$$

with homogeneous Neumann boundary condition $\nabla u \cdot \vec{\nu} = 0$ along $\partial\Omega$. Here $I_2 \in \mathbb{R}^{2\times 2}$ is the identity matrix, $\vec{n}$ is the normal vector of $\partial\Omega$, and $\Phi'(\kappa_\beta(u))$ is the derivative of $\Phi(\kappa_\beta(u))$. Below we shall take $\Phi(\kappa_\beta(u)) = \kappa_\beta(u)^2$, so $\Phi'(\kappa_\beta(u)) = 2\kappa_\beta(u)$ and $\nabla\Phi'(\kappa_\beta(u)) = 2\nabla\kappa_\beta(u)$.

The selection of β plays an important role in numerical implementations since $\beta \ll 1$ will lead to the Euler–Lagrange equation of (5) too stiff to solve by numerical continuation. To deal with this problem, β will be used as a homotopy

parameter and the numerical continuation we present here allows us to reach a relatively small value for β, still maintaining good performance (see [24,18,20]).

Although Newton's method as a standard unconstrained optimization method is a preferred method, it does not work satisfactorily for our PDE problem, due to high nonlinearity, in the sense that its domain of convergence is very small when β is small, which requires an initial guess (better than the noisy image f and) close to the true solution (see [42,34,3,9,19, 37]). Refer to [16,33] for theoretical work on the radius of convergence of Newton method for denoising models. Standard fixed point methods and primal–dual methods are usually fast algorithms for the TV denoising model, but they do not converge for this mean curvature-based model. Only two methods have been proposed to solve Eq. (6) (see [6,7,46]).

(1) *Gradient descent methods*. As used in [46], instead of the elliptic PDE, a parabolic PDE with time as an evolution parameter is solved by the gradient descent method

$$u_t = -\alpha\nabla\cdot\left(\frac{1}{|\nabla u|_\beta}\left(I_2 - \frac{\nabla u\nabla u^T}{|\nabla u|_\beta^2}\right)\nabla\Phi'\big(\kappa_\beta(u)\big)\right) - (u-f), \tag{7}$$

with $u(x,y,0) = f$. This method is preferred in many situations for its simplicity and fast initial convergence, but its overall convergence is slow (or the time step must be small for stability) to reach steady state since the parabolic term is nearly singular for small gradients.

(2) *Stabilized fixed point method and nonlinear multigrid*. The idea of stabilized fixed point method is to split the Euler–Lagrange equation (6) in two parts (convex and nonconvex) and treat the convex part implicitly and the nonconvex part explicitly, after adding suitable stabilizing terms. Thus, the stabilized fixed point method of [6] takes the form

$$\begin{aligned} &-\gamma\nabla\cdot\frac{\nabla u^{(k+1)}}{|\nabla u^{(k)}|_\beta} - \alpha\nabla\cdot\left(\frac{\nabla u^{(k)}\cdot\nabla\Phi'(\kappa_\beta(u^{(k)}))}{|\nabla u^{(k)}|_\beta^3}\nabla u^{(k+1)}\right) + u^{(k+1)} \\ &\quad = -\gamma\nabla\cdot\frac{\nabla u^{(k)}}{|\nabla u^{(k)}|_\beta} - \alpha\nabla\cdot\frac{\nabla\Phi'(\kappa_\beta(u^{(k)}))}{|\nabla u^{(k)}|_\beta} + f. \end{aligned} \tag{8}$$

Further an efficient nonlinear multigrid for (6) is developed using this stabilized fixed point method as a smoother. Although stabilization helps to derive a convergent fixed point method, the smoothing parameter β in (8) cannot be small, and was typically chosen to be, say, 10^{-2} or larger. Our new methods below will allow small β in (6) (e.g. $\beta < 10^{-6}$).

As mentioned, if the original functional (5) is approximated by a new functional [44,23], the fourth order PDE will be reduced to second order ones. We will tackle the PDE (6) directly and not pursue this alternative route. We also remarked that there are competing models other than (6) for improving the TV model [5,8,28].

3. A fixed point curvature method

In the curvature model (5), we take $\Phi(\kappa_\beta(u)) = \kappa_\beta(u)^2$ as an example [46]. As remarked, all known fixed point methods do not work for the model. Here we introduce a fixed point curvature method that converges for the Euler–Lagrange equation (6). Other curvature models e.g. $\Phi(\kappa_\beta(u)) = |\kappa_\beta(u)|$ may be considered similarly.

Solution of the TV model. Before our new method is presented, we briefly review the minimization of the TV model [38,11], defined by

$$\min_u\left\{E(u) = \alpha\int_\Omega |\nabla u|\,dx\,dy + \frac{1}{2}\|u-f\|^2\right\}, \tag{9}$$

whose Euler–Lagrange equation is the second order equation

$$F(u) = -\alpha\nabla\cdot\frac{\nabla u}{|\nabla u|_\beta} + (u-f) = 0. \tag{10}$$

Much theoretical work on this TV model has been done in recent years [11,42,34,1,40,4]. The solution u to this model lies in the space of functions with bounded variation $\mathrm{BV}(\Omega)$; see [40].

In Newton's method, the lagged fixed point method and the primal–dual methods, a descent direction must be computed to obtain the new iterate $u^{(k+1)}$ using the current iterate $u^{(k)}$ (see [41,42,13]). The first two are based on solving (10) directly for the primal variable u, and the third introduces a new (dual) variable $w = \frac{\nabla u}{|\nabla u|_\beta}$ and replaces (10) by the following system of nonlinear partial differential equations

$$\begin{aligned} F(u,w) &= -\alpha\nabla\cdot w + (u-f) = 0, \\ G(u,w) &= w|\nabla u|_\beta - \nabla u = 0. \end{aligned}$$

Setting $\delta u^{(k)} = u^{(k+1)} - u^{(k)}$, the linearization systems of the Newton method, the lagged fixed point method and the primal–dual method are as follows:

(1) *Newton method*

$$\left[-\alpha\nabla\cdot\left(\frac{1}{|\nabla u^{(k)}|_\beta}\left(I_2 - \frac{\nabla u^{(k)}(\nabla u^{(k)})^T}{|\nabla u^{(k)}|_\beta^2}\right)\nabla\right) + 1\right]\delta u^{(k)} = -F\big(u^{(k)}\big).$$

(2) *Lagged fixed point method*

$$\left[-\alpha\nabla\cdot\left(\frac{1}{|\nabla u^{(k)}|_\beta}\nabla\right) + 1\right]\delta u^{(k)} = -F\big(u^{(k)}\big).$$

(3) *Primal–dual method*

$$\begin{bmatrix} -\alpha\nabla\cdot & 1 \\ |\nabla u^{(k)}|_\beta I_2 & -(I_2 - \frac{w^{(k)}(\nabla u^{(k)})^T}{|\nabla u^{(k)}|_\beta})\nabla \end{bmatrix}\begin{bmatrix} \delta w^{(k)} \\ \delta u^{(k)} \end{bmatrix} = -\begin{bmatrix} F(u^{(k)}, w^{(k)}) \\ G(u^{(k)}, w^{(k)}) \end{bmatrix}.$$

The descent direction $\delta u^{(k)}$ for $E(u)$ is obtained by solving

$$\left[-\alpha\nabla\cdot\left(\frac{1}{|\nabla u^{(k)}|_\beta}\left(I_2 - \frac{w^{(k)}(\nabla u^{(k)})^T}{|\nabla u^{(k)}|_\beta}\right)\nabla\right) + 1\right]\delta u^{(k)} = -F\big(u^{(k)}\big)$$

and

$$\delta w^{(k)} = \frac{1}{|\nabla u^{(k)}|_\beta}\left(I_2 - \frac{w^{(k)}(\nabla u^{(k)})^T}{|\nabla u^{(k)}|_\beta}\right)\nabla\delta u^{(k)} - w^{(k)} + \frac{\nabla u^{(k)}}{|\nabla u^{(k)}|_\beta}.$$

Clearly all three methods take the linearized form

$$\big(\alpha M_\beta\big(u^{(k)}\big) + 1\big)\delta u^{(k)} = -F\big(u^{(k)}\big),$$

where $u^{(k)}$ is a previous iterate and $M_\beta(u)$ denotes respectively the following

Newton method $\quad M_\beta^{\mathrm{N}}(u) = -\nabla\cdot\left(\frac{1}{|\nabla u|_\beta}\left(I_2 - \frac{\nabla u\nabla u^T}{|\nabla u|_\beta^2}\right)\nabla\right),$

Lagged fixed point method $\quad M_\beta^{\mathrm{FP}}(u) = -\nabla\cdot\left(\frac{1}{|\nabla u|_\beta}\nabla\right),$

Primal–dual method $\quad M_\beta^{\mathrm{PD}}(u) = -\nabla\cdot\left(\frac{1}{|\nabla u|_\beta}\left(I_2 - \frac{w\nabla u^T}{|\nabla u|_\beta}\right)\nabla\right).$

Solution of the curvature model. Our idea is motivated by the observation that the fourth order nonlinear operator of Euler–Lagrange equation (6) can be considered as a second order nonlinear operator compounding another second order nonlinear operator, therefore, (6) can be rewritten as

$$\begin{aligned} g_\beta(u) &= 2\alpha\left(\nabla\cdot\left(\frac{1}{|\nabla u|_\beta}\left(I_2 - \frac{\nabla u\nabla u^T}{|\nabla u|_\beta^2}\right)\nabla\right)\right)\left(\nabla\cdot\frac{\nabla u}{|\nabla u|_\beta}\right) + (u - f) \\ &= 2\alpha M_\beta^{\mathrm{N}}(u)\left(-\nabla\cdot\frac{\nabla u}{|\nabla u|_\beta}\right) + (u - f) = 0. \end{aligned} \tag{11}$$

Thus, our FP equation is obtained by freezing the nonlinearity of the first second order nonlinear operator $2\alpha M_\beta^{\mathrm{N}}(u)$ at a known iterate $u^{(l,0)}$, with (11) becoming

$$g_\beta\big(u^{(l,0)}, u\big) = 2\alpha M_\beta^{\mathrm{N}}\big(u^{(l,0)}\big)\left(-\nabla\cdot\frac{\nabla u}{|\nabla u|_\beta}\right) + (u - f) = 0. \tag{12}$$

Notice that the original PDE (11) has its nonlinearity formed from multiplying a nonlinear operator $2\alpha M_\beta^{\mathrm{N}}(u)$ to another nonlinear one. In contrast, our new FP equation (12) is also a fourth order nonlinear partial differential equation but the nonlinearity is reduced, now consisting of a linear operator $2\alpha M_\beta^{\mathrm{N}}(u^{(l,0)})$ multiplying a nonlinear one. The reduced nonlinearity in (12) will enable us to construct a converging homotopy method for (11) and the details remain to discuss.

Now we describe the discretization of the continuous formulation of the fixed point curvature method and also define the notation used throughout the report. Let $\Omega = [0,1] \times [0,1]$ with mesh size $h = 1/n$, containing n^2 pixels (i,j), for $i,j = 1,2,\ldots,n$, and $u_{i,j}$ represent the value of the function u at pixel (i,j), then the discrete gradient operator at pixel (i,j) is

$$(\nabla u)_{i,j} = \big((u_x)_{i,j}, (u_y)_{i,j}\big)$$

with

$$(u_x)_{i,j} = \frac{1}{h}\begin{cases} u_{i+1,j} - u_{i,j} & \text{if } i < n, \\ 0 & \text{if } i = n, \end{cases} \qquad (u_y)_{i,j} = \frac{1}{h}\begin{cases} u_{i,j+1} - u_{i,j} & \text{if } j < n, \\ 0 & \text{if } j = n. \end{cases}$$

The discrete divergence operator is the negative adjoint of the gradient operator from the analysis of the continuous setting, namely $\nabla\cdot = -\nabla^*$. Therefore, it can be defined as follows:

$$(\nabla \cdot w)_{i,j} = \frac{1}{h}\begin{cases} (w_1)_{i,j} - (w_1)_{i-1,j} & \text{if } 1 < i < n \\ (w_1)_{i,j} & \text{if } i = 1 \\ -(w_1)_{i-1,j} & \text{if } i = n \end{cases} + \frac{1}{h}\begin{cases} (w_2)_{i,j} - (w_2)_{i,j-1} & \text{if } 1 < j < n \\ (w_2)_{i,j} & \text{if } j = 1 \\ -(w_2)_{i,j-1} & \text{if } j = n. \end{cases}$$

For ease of the notation, since α is a parameter to be chosen, we drop h from now on without loss of generality and loss of accuracy; refer also to [6,44,23,10,35,45]. Once we stack the grid functions u along rows of Ω into a vector

$$\mathbf{u} = (u_{1,1},\ldots,u_{n,1},u_{1,2},\ldots,u_{n,2},\ldots,u_{1,n},\ldots,u_{n,n})^T,$$

as commonly done, then $\mathbf{u} \in \mathbb{R}^N$, where $N = n^2$. The discrete gradient $(\nabla u)_{i,j}$ can be expressed by a multiplication of the matrix $A_l^T \in \mathbb{R}^{2\times N}$, for $l = 1,2,\ldots,N$, to the vector $\mathbf{u}$:

$$A_l^T\mathbf{u} = \begin{cases} (\mathbf{u}_{l+1} - \mathbf{u}_l; \mathbf{u}_{l+n} - \mathbf{u}_l) & \text{if } l \bmod n \neq 0 \text{ and } l+n \leqslant N, \\ (0; \mathbf{u}_{l+n} - \mathbf{u}_l) & \text{if } l \bmod n = 0 \text{ and } l+n \leqslant N, \\ (\mathbf{u}_{l+1} - \mathbf{u}_l; 0) & \text{if } l \bmod n \neq 0 \text{ and } l+n > N, \\ (0;0) & \text{if } l \bmod n = 0 \text{ and } l+n > N. \end{cases}$$

We also stack the grid functions $A_l^T\mathbf{u}$ along rows into a vector. We form the matrix A by concatenating the matrices A_l, $l = 1,2,\ldots,N$, that is,

$$A = (A_1,\ldots,A_N) \in \mathbb{R}^{N\times 2N}.$$

In this notation, the divergence $\nabla\cdot\nabla u$ is simply $-\sum_i A_i(A_i^T\mathbf{u})$. Denoted by $M_\beta^{\mathrm{N}}(\mathbf{u})$, $M_\beta^{\mathrm{FP}}(\mathbf{u})$, $M_\beta^{\mathrm{PD}}(\mathbf{u})$, $M_\beta(\mathbf{u})$, $g_\beta(\mathbf{u})$, and $g_\beta(\mathbf{u}^{(l,0)},\mathbf{u})$ the discretization of $M_\beta^{\mathrm{N}}(u)$, $M_\beta^{\mathrm{FP}}(u)$, $M_\beta^{\mathrm{PD}}(u)$, $M_\beta(u)$, $g_\beta(u)$, and $g_\beta(u^{(l,0)},u)$, respectively, then

$$M_\beta^{\mathrm{N}}(\mathbf{u}) = \sum_i A_i\left[\frac{1}{|A_i^T\mathbf{u}|_\beta}\left(I_{2N} - \frac{A_i^T\mathbf{u}\otimes(A_i^T\mathbf{u})^T}{|A_i^T\mathbf{u}|_\beta^2}\right)A_i^T\right],$$

$$M_\beta^{\mathrm{FP}}(\mathbf{u}) = \sum_i A_i\left(\frac{A_i^T}{|A_i^T\mathbf{u}|_\beta}\right),$$

$$M_\beta^{\mathrm{PD}}(\mathbf{u}) = \sum_i A_i\left[\frac{1}{|A_i^T\mathbf{u}|_\beta}\left(I_{2N} - \frac{\mathbf{w}\otimes(A_i^T\mathbf{u})^T}{|A_i^T\mathbf{u}|_\beta}\right)A_i^T\right],$$

where $I_{2N} \in \mathbb{R}^{2N\times 2N}$ is an identity matrix. The discretizations of (11) and (12) are

$$g_\beta(\mathbf{u}) = 2\alpha M_\beta^{\mathrm{N}}(\mathbf{u})\left(\sum_j A_j\left(\frac{A_j^T\mathbf{u}}{|A_j^T\mathbf{u}|_\beta}\right)\right) + (\mathbf{u}-\mathbf{f}) = 0, \tag{13}$$

$$g_\beta\big(\mathbf{u}^{(l,0)},\mathbf{u}\big) = 2\alpha M_\beta^{\mathrm{N}}\big(\mathbf{u}^{(l,0)}\big)\left(\sum_j A_j\left(\frac{A_j^T\mathbf{u}}{|A_j^T\mathbf{u}|_\beta}\right)\right) + (\mathbf{u}-\mathbf{f}) = 0. \tag{14}$$

Here (14) is still nonlinear. It can be successively linearized as

$$\begin{aligned}&\big[2\alpha M_\beta^{\mathrm{N}}\big(\mathbf{u}^{(l,0)}\big)M_\beta\big(\mathbf{u}^{(l,k)}\big) + I_N\big]\big(\mathbf{u}-\mathbf{u}^{(l,k)}\big) + g_\beta\big(\mathbf{u}^{(l,0)},\mathbf{u}^{(l,k)}\big)\\ &\quad = \tilde{M}_\beta\big(\mathbf{u}^{(l,0)},\mathbf{u}^{(l,k)}\big)\big(\mathbf{u}-\mathbf{u}^{(l,k)}\big) + g_\beta\big(\mathbf{u}^{(l,0)},\mathbf{u}^{(l,k)}\big) = 0, \quad k = 0,1,2,\ldots\end{aligned} \tag{15}$$

where $I_N \in \mathbb{R}^{N\times N}$ is an identity matrix and $M_\beta(\mathbf{u}^{(l,k)})$ can be one of these three operators

$$M_\beta^{\mathrm{N}}\big(\mathbf{u}^{(l,k)}\big), \qquad M_\beta^{\mathrm{FP}}\big(\mathbf{u}^{(l,k)}\big), \qquad M_\beta^{\mathrm{PD}}\big(\mathbf{u}^{(l,k)}\big),$$

corresponding to the use of the Newton method, the lagged fixed point method, and the primal–dual method respectively. Although such a notation includes three separate methods, our recommendation will be the third choice for a fixed point curvature method with primal–dual iterations.

We now address the solvability of (15) and will show $\tilde{M}_\beta(\mathbf{u}^{(l,0)}, \mathbf{u}^{(l,k)})$ is a positive definite matrix by the following two propositions.

Proposition 1. *The matrices $M_\beta^{\mathrm{N}}(\mathbf{u})$ and $M_\beta^{\mathrm{FP}}(\mathbf{u})$ are symmetric positive semidefinite, and $M_\beta^{\mathrm{PD}}(\mathbf{u})$ is positive semidefinite if $|\mathbf{w}_i| \leqslant 1$ at all grid points.*

Proof. For any $\mathbf{v} \in \mathbb{R}^N$, we have

$$M_\beta^{\mathrm{N}}(\mathbf{u})(\mathbf{v},\mathbf{v}) = \sum_i \frac{1}{|A_i^T\mathbf{u}|_\beta}\left(\big|A_i^T\mathbf{v}\big|^2 - \frac{(A_i^T\mathbf{u}, A_i^T\mathbf{v})^2}{|A_i^T\mathbf{u}|_\beta^2}\right).$$

It is clear that $|A_i^T\mathbf{v}|^2 - \frac{(A_i^T\mathbf{u}, A_i^T\mathbf{v})^2}{|A_i^T\mathbf{u}|_\beta^2} \geqslant 0$ for any $\beta > 0$, then, $M_\beta^{\mathrm{N}}(\mathbf{u})(\mathbf{v},\mathbf{v}) \geqslant 0$, and $M_\beta^{\mathrm{N}}(\mathbf{u}) = (M_\beta^{\mathrm{N}}(\mathbf{u}))^T$, so the matrix $M_\beta^{\mathrm{N}}(\mathbf{u})$ is symmetric positive semidefinite. By a similar procedure we can prove $M_\beta^{\mathrm{FP}}(\mathbf{u})$ and $M_\beta^{\mathrm{PD}}(\mathbf{u})$ are positive semidefinite matrices. □

Proposition 2. *If $A \in \mathbb{R}^{N\times N}$ is a symmetric positive semidefinite matrix and $B \in \mathbb{R}^{N\times N}$ is a positive semidefinite matrix, then the eigenvalues of the product of these two matrices are nonnegative.*

Proof. By the assumption that A is a symmetric positive semidefinite matrix, then there exists a matrix $C \in \mathbb{R}^{N\times N}$, such that $A = CC^T$.

We will prove $AB = CC^TB$ and C^TBC share the same eigenvalues by proving they have the same characteristic polynomial. The proof starts by computing

$$\begin{pmatrix} I_N & -C \\ \mathbf{0} & \lambda I_N \end{pmatrix}\begin{pmatrix} C & \lambda I_N \\ I_N & C^TB \end{pmatrix} = \begin{pmatrix} \mathbf{0} & \lambda I_N - CC^TB \\ \lambda I_N & \lambda C^TB \end{pmatrix}. \tag{16}$$

By taking determinant of both sides in (16), we obtain

$$\lambda^N \begin{vmatrix} C & \lambda I_N \\ I_N & C^TB \end{vmatrix} = \lambda^N(-1)^N\big|\lambda I_N - CC^TB\big|. \tag{17}$$

Similarly, since

$$\begin{pmatrix} I_N & \mathbf{0} \\ -C^TB & \lambda I_N \end{pmatrix}\begin{pmatrix} C & \lambda I_N \\ I_N & C^TB \end{pmatrix} = \begin{pmatrix} C & \lambda I_N \\ \lambda I_N - C^TBC & \mathbf{0} \end{pmatrix}, \tag{18}$$

we have

$$\lambda^N \begin{vmatrix} C & \lambda I_N \\ I_N & C^TB \end{vmatrix} = \lambda^N(-1)^N\big|\lambda I_N - C^TBC\big|. \tag{19}$$

Comparing (17) with (19), we can draw the conclusion that

$$\big|\lambda I_N - CC^TB\big| = \big|\lambda I_N - C^TBC\big|,$$

namely, $AB = CC^TB$ and C^TBC have the same characteristic polynomial.

If we can prove the eigenvalues of the matrix C^TBC are nonnegative, then we arrive at our conclusion. For any given vector x, set $y = Cx$, since B is a positive semidefinite matrix, then $y^TBy \geqslant 0$, namely $x^TC^TBCx \geqslant 0$. Since x is any given vector, then C^TBC is a positive semidefinite matrix. Therefore, the eigenvalues of C^TBC and hence those of AB are nonnegative. □

From Propositions 1 and 2, we know the eigenvalues of $M_\beta^{\mathrm{N}}(\mathbf{u}^{(l,0)})M_\beta(\mathbf{u}^{(l,k)})$ are nonnegative. Therefore,

$$\tilde{M}_\beta\big(\mathbf{u}^{(l,0)}, \mathbf{u}^{(l,k)}\big) = 2\alpha M_\beta^{\mathrm{N}}\big(\mathbf{u}^{(l,0)}\big)M_\beta\big(\mathbf{u}^{(l,k)}\big) + I_N$$

is a positive definite matrix. Clearly, all eigenvalues are larger than or equal to 1, which guarantees the existence of

$$\delta\mathbf{u}^{(l,k)} = -\tilde{M}_\beta\big(\mathbf{u}^{(l,0)}, \mathbf{u}^{(l,k)}\big)^{-1} g_\beta\big(\mathbf{u}^{(l,0)}, \mathbf{u}^{(l,k)}\big).$$

Moreover, the linear system $\tilde{M}_\beta(\mathbf{u}^{(l,0)}, \mathbf{u}^{(l,k)})\delta\mathbf{u}^{(l,k)} = -g_\beta(\mathbf{u}^{(l,0)}, \mathbf{u}^{(l,k)})$ can be solved by suitable iterative solvers; here we use a preconditioned conjugate gradient method.

From [42,13,34,31,16], for the TV equation (10), the lagged fixed point method and the primal–dual method converge for any nonzero β. However, the Newton method only converges for large β. For the curvature equation (14), the same observations can be made. But we hope to use a Newton type method whenever possible. To achieve this, we require a homotopy algorithm. For now, assuming that a good initial solution $\mathbf{u}^{(0,0)}$ is available, we simply describe how (13) will be solved in preparation for a homotopy algorithm.

Algorithm 1. $[\mathbf{u}, l, flag] \leftarrow EL\_solver(\mathbf{u}^{(0,0)}, \mathbf{f}, tol_1, tol, maxit_1, maxit, \alpha, \beta)$

Step 1. Compute $J_\beta(\mathbf{u}^{(0,0)})$ and set $l := 1$.
Step 2. $[\mathbf{u}^{(l,0)}, iter, flag] \leftarrow FP\_solver(\mathbf{u}^{(l-1,0)}, \mathbf{f}, tol, maxit, \alpha, \beta)$.
Compute the energy function $J_\beta(\mathbf{u}^{(l,0)})$.
Step 3. If $|J_\beta(\mathbf{u}^{(l,0)}) - J_\beta(\mathbf{u}^{(l-1,0)})| < tol_1$ or $l = maxit_1$, then
return with $\mathbf{u} = \mathbf{u}^{(l,0)}$.
Else set $l = l + 1$, then return to Step 2.

The *FP_solver* in Step 2 of Algorithm 1 is the following.

Algorithm 2. $[\mathbf{u}, k, flag] \leftarrow FP\_solver(\mathbf{u}^{(l,0)}, \mathbf{f}, tol, maxit, \alpha, \beta)$

Step 1. Set $k := 0$, $flag := 1$, compute $M_\beta^{\mathrm{N}}(\mathbf{u}^{(l,0)})$, $g_\beta(\mathbf{u}^{(l,0)}, \mathbf{u}^{(l,0)})$, and $res_0 := \|g_\beta(\mathbf{u}^{(l,0)}, \mathbf{u}^{(l,0)})\|_2$.
Step 2. Choose one linear operator for $g_\beta(\mathbf{u}^{(l,0)}, \mathbf{u})$ to compute $\tilde{M}_\beta(\mathbf{u}^{(l,0)}, \mathbf{u}^{(l,k)})$, $\mathbf{u}^{(l,k+1)} = \mathbf{u}^{(l,k)} - \tilde{M}_\beta(\mathbf{u}^{(l,0)}, \mathbf{u}^{(l,k)})^{-1} \times g_\beta(\mathbf{u}^{(l,0)}, \mathbf{u}^{(l,k)})$, and $k = k + 1$.
Step 3. Compute $g_\beta(\mathbf{u}^{(l,0)}, \mathbf{u}^{(l,k)})$, then set $relres := \|g_\beta(\mathbf{u}^{(l,0)}, \mathbf{u}^{(l,k)})\|_2 / res_0$.
Step 4. If $relres \leqslant tol$, then
record the iteration, then return $\mathbf{u} = \mathbf{u}^{(l,k)}$ (solution has been found).
Else
if the *maxit* iterations have been performed, then
set $\mathbf{u} = \mathbf{u}^{(l,0)}$ and $flag = 0$.
Else return to Step 2.

In summary, since the fixed point curvature method via Algorithm 1 uses $\mathbf{u}^{(0,0)} = \mathbf{f}$ at the very first iteration, the following $\mathbf{u}^{(l+1,0)}$ is the solution of $g_\beta(\mathbf{u}^{(l,0)}, \mathbf{u}) = 0$. The whole process consists of a succession of the following two steps.

1. Solve $g_\beta(\mathbf{u}^{(l,0)}, \mathbf{u}) = 0$ by Algorithm 2, and denote its solution by $\mathbf{u}^{(l+1,0)}$.
2. Set $l = l + 1$ and continue iterations till termination by some tolerance.

4. Homotopy method for the curvature Euler–Lagrange equation

A homotopy method offers a convergent solution for a large class of nonlinear equations. As a globally convergent method, the homotopy method has versatility and robustness, and has become an important tool for solving nonlinear problems; see [24,18,20,2,27,43]. The basic idea of a homotopy algorithm is to construct a continuous map $H(\mathbf{u}, t)$ with parameter t which deforms a simple function $H(\mathbf{u}, 0)$ to the given function $H(\mathbf{u}, 1)$ as t varies from 0 to 1.

To find a required solution from tracking the solution curve Γ emanating from the solution of $H(\mathbf{u}, 0) = 0$, the homotopy algorithm requires Γ obey strict smoothness conditions. There are many continuous maps that can satisfy these conditions. For example, to solve (13), the following simple homotopy

$$H(\mathbf{u}, t) = tg_\beta(\mathbf{u}) + (1-t)(\mathbf{u} - \mathbf{f}) = 2t\alpha M_\beta^{\mathrm{N}}(\mathbf{u})\left(\sum_j A_j\left(\frac{A_j^T\mathbf{u}}{|A_j^T\mathbf{u}|_\beta}\right)\right) + (\mathbf{u} - \mathbf{f}) = 0$$

can be considered. However, the singularity and nonlinearity of $H(\mathbf{u}, t) = 0$ is the same as that of (13) even for t not near 1.

To construct a better homotopy for solving (13), we hope to reduce its level of singularity and nonlinearity when t is not near 1. Our suggested homotopy map is as follows

$$H(\mathbf{u},t)=2\alpha\sum_i A_i\left[\frac{1}{|A_i^T\mathbf{u}|_{\beta(t)}}\left(I_{2N}-\frac{A_i^T\mathbf{u}\otimes(A_i^T\mathbf{u})^T}{|A_i^T\mathbf{u}|^2_{\beta(t)}}\right)A_i^T\right]\left[\sum_j A_j\left(\frac{A_j^T\mathbf{u}}{|A_j^T\mathbf{u}|_{\beta(t)}}\right)\right]+(\mathbf{u}-\mathbf{f})=0, \tag{20}$$

where $\beta(t)=(1-t)/t^2$, $t\in(0,1]$. When $t>0$ is small, $\beta(t)$ is large and the level of singularity and nonlinearity of $H(\mathbf{u},t)=0$ is lower than (13), and easier to solve. Other choices of $\beta(t)$ may be permitted as long as they ensure a positive and monotonically decreasing $\beta(t)$ such that $\beta(1)=0$ and $\beta(t_0)>0$ is large when $t_0\approx 0$. To allow $t=0$, rewrite Eq. (20) as

$$\begin{aligned}H(\mathbf{u},t)=2\alpha\sum_i A_i&\left[\frac{t}{\sqrt{t^2|A_i^T\mathbf{u}|^2+(1-t)}}\left(I_{2N}-\frac{t^2A_i^T\mathbf{u}\otimes(A_i^T\mathbf{u})^T}{t^2|A_i^T\mathbf{u}|^2+(1-t)}\right)A_i^T\right]\\&\cdot\left[\sum_j A_j\left(\frac{tA_j^T\mathbf{u}}{\sqrt{t^2|A_j^T\mathbf{u}|^2+(1-t)}}\right)\right]+(\mathbf{u}-\mathbf{f})=0,\end{aligned} \tag{21}$$

since

$$\frac{1}{|A_i^T\mathbf{u}|_{\beta(t)}}=\frac{1}{\sqrt{|A_i^T\mathbf{u}|^2+(1-t)/t^2}}=\frac{t}{\sqrt{t^2|A_i^T\mathbf{u}|^2+(1-t)}}. \tag{22}$$

Here $H(\mathbf{u},0)=\mathbf{u}-\mathbf{f}$ implies that our initial solution is the given image (as commonly used in denoising algorithms) and $H(\mathbf{u},1)=0$ will give the solution for (13) with $\beta=0$.

We can solve a sequence of equations $H(\mathbf{u},t_k)=0$ for adaptively increasing t_k up to 1 (in practice, we will stop at certain $t_*<1$ near 1 such that $\beta(t_*)=\beta$, a prescribed small enough smooth parameter). The solution of $H(\mathbf{u},t_{k-1})=0$ serves as the good initial guess for iteratively solving $H(\mathbf{u},t_k)=0$. The whole process is a special predictor–corrector path following procedure with a staircase predictor. The technique consists of the following two phases.

- *Predictor step*. For $t_0=0$, the solution of $H(\mathbf{u},t_0)=0$ is known, namely $\mathbf{u}^0=\mathbf{f}$. After we have obtained an approximate solution $\mathbf{u}^{k-1}$ of $H(\mathbf{u},t_{k-1})=0$ for some $t_{k-1}\in[0,1)$, increase t with some predictor steplength θ_{k-1} to reach $t_k=t_{k-1}+\theta_{k-1}$ and the solution of $H(\mathbf{u},t_k)=0$ is provided with the initial guess $\mathbf{u}^{k-1}$.
- *Corrector steps*. From the initial point $\mathbf{u}^{k-1}$, approximately solve $H(\mathbf{u},t_k)=0$ by the fixed point curvature method. Because the parameter t is introduced into Eq. (21) to compute $1/|A_i^T\mathbf{u}|_{\beta(t)}$, the fixed point curvature method used here is slightly different from Algorithms 1 and 2 in replacing the parameter $\beta=\beta(t)$ by t. If θ_{k-1} is suitably chosen, $\mathbf{u}^{k-1}$ will be close to the solution of $H(\mathbf{u},t_k)=0$, and hence, the convergence of the fixed point curvature method is assured.

As we know, the prediction phases and the correction phases mutually affect each other. The predictor steplength θ is adjusted according to the performance of the corrector procedure as done below in Algorithm 3. When a corrector step terminates within prescribed steps of *iter*1, θ is considered too small for the next predictor and is increased, when the iterations terminate over some *iter*2 > *iter*1 steps and converge, θ is considered too large and will be decreased, while if the iterations diverge, the predictor–corrector step is abandoned and then is restarted starting with a smaller θ. The predictor–corrector path following procedure is shown as follows:

Algorithm 3 *(Homotopy method).* $\mathbf{u}\leftarrow homotopy(\mathbf{f}, tol_1, tol, maxit_1, maxit, \theta, \alpha, \beta)$

Step 1. Set $k=1$, $\mathbf{u}^{k-1}:=\mathbf{f}$ and $t_{k-1}:=0$.
Step 2. Set $t_k:=t_{k-1}+\theta$.
If $t_k\geqslant 2/(1+\sqrt{1+4\beta})$, then
$t_k=2/(1+\sqrt{1+4\beta})$,
$[\mathbf{u}^k, iter, flag]\leftarrow EL\_solver(\mathbf{u}^{k-1},\mathbf{f}, tol_1, tol, maxit_1, maxit, \alpha, t_k)$.
If $flag=1$, then
return $\mathbf{u}=\mathbf{u}^k$ (solution has been found).
Else set $\theta=\theta/2$, $t_k=t_{k-1}+\theta(1-t_{k-1})$.
Step 3. $[\mathbf{u}^k, iter, flag]\leftarrow EL\_solver(\mathbf{u}^{k-1},\mathbf{f}, tol_1, tol, maxit_1, maxit, \alpha, t_k)$.
if $flag=1$, then
set $k=k+1$.
If the iteration count *iter* is less than *iter*1, then
increase θ by $\theta:=1.2\theta$.
If the iteration count *iter* is more than *iter*2, then
reduce θ slightly by $\theta:=\theta/1.2$.

Return to Step 2.
Else reduce θ by $\theta := \theta/2$.
If θ is unreasonably small, then
return with an error Flag.
Else return to Step 2.

5. Numerical experiments and discussions

In this section we test our restoration algorithms on several images of 2 resolutions, 128×128, 256×256 and 512×512 pixels, with an intensity range of $[0, 255]$. Energy values of the minimizing functional from (5), the signal to noise ratio (SNR), the peak signal to noise ratio (PSNR), and the difference between a digital image and its denoised version are used to measure the quality of the restored images, and we define the latter three by

$$\mathrm{SNR} = \frac{\sum_{i=1}^{n}\sum_{j=1}^{n} u_{i,j}^2}{\sum_{i=1}^{n}\sum_{j=1}^{n}(u_{i,j}-\tilde{u}_{i,j})^2}, \qquad \mathrm{PSNR} = 10\log_{10}\frac{255^2}{\frac{1}{n^2}\sum_{i=1}^{n}\sum_{j=1}^{n}(u_{i,j}-\tilde{u}_{i,j})^2},$$

and

$$\mathrm{diff}(\tilde{u}) = \tilde{u} - f,$$

where u, $\tilde{u}$ and f are respectively the original image, the restored image and the noisy image.

Below we shall refer to the method of Algorithm 1 with a fixed β (with Algorithm 2 by a primal–dual method) as our fixed point curvature method. As such, in following figures, "Inner iterations" will mean the "number of accumulated primal–dual iterations" for the fixed point curvature method, and the homotopy method.

5.1. Comparisons of our fixed point curvature method with our homotopy method

In this section, we use a 128×128 "triangle" contaminated with zero mean Gaussian random noise (see Fig. 1) as the test image. The denoised images by the fixed point curvature method and our homotopy method can be seen in Figs. 6 and 7 respectively. Fig. 2 shows $maxit_1 = 1$ is slightly better than $maxit_1 = 2$ when we take $\beta = 10^{-6}$ in our homotopy method, so we use $maxit_1 = 1$ in the following tests.

- *α-dependence test*. Here we analyze how sensitive the performance of our fixed point curvature method and our homotopy method is when $\alpha = 50$, 100, 150, 200, while $\beta = 1$ is unchanged. We can see a clear process of the changes of SNR using fixed point curvature method and homotopy method with different α in Fig. 3. Although both of them improve the quality of the image for the different values of α, we see that the performance of our fixed point curvature method for $\alpha = 50$ is less efficient while the homotopy method is more consistently behaved.
- *β-dependence test*. After the analysis of the effect of α, we analyze how β affects the performance of fixed point curvature method and homotopy method. Here we take $\alpha = 150$ and vary $\beta = 1$, 10^{-2}, 10^{-6}, 10^{-8}. Fig. 4 shows the history of SNR using fixed point curvature method and homotopy method with different β. Obviously, both of them improve the quality of the image for the different values of β and as expected the number of the iterations is increased when β is small. We can also observe the quality of the image recovered by Algorithm 1 is somewhat sensitive as β reduces, but the homotopy method is not.

Fig. 5 shows the comparisons of the number of accumulated primal–dual iterations, SNR, and energy value between fixed point curvature method and homotopy method with $\alpha = 150$, $\beta = 10^{-4}$. We can draw the conclusion that our homotopy method is faster and more robust than our fixed point curvature method.

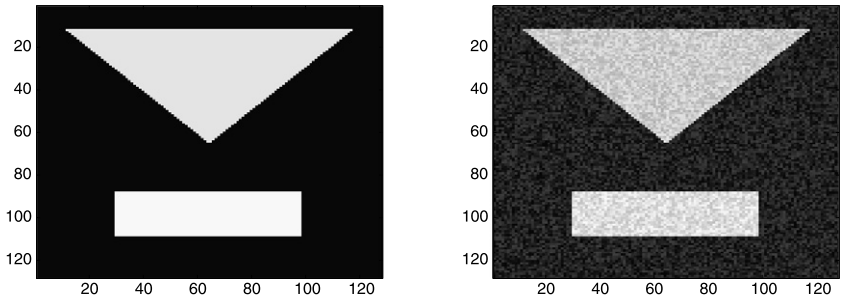

Fig. 1. The original "triangle" image (left) and noisy image (right).

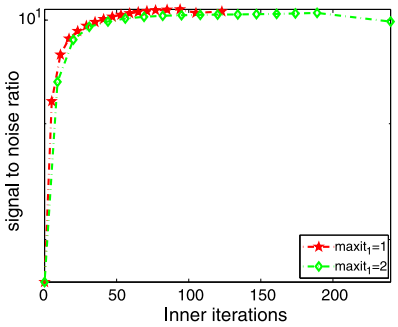

Fig. 2. The comparison of the correction phase using $maxit_1 = 1$ and $maxit_1 = 2$.

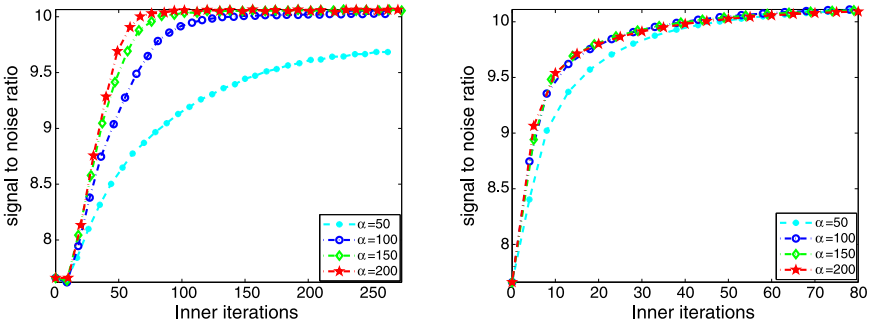

Fig. 3. Comparisons of fixed point curvature method (left) and homotopy method (right) for different α.

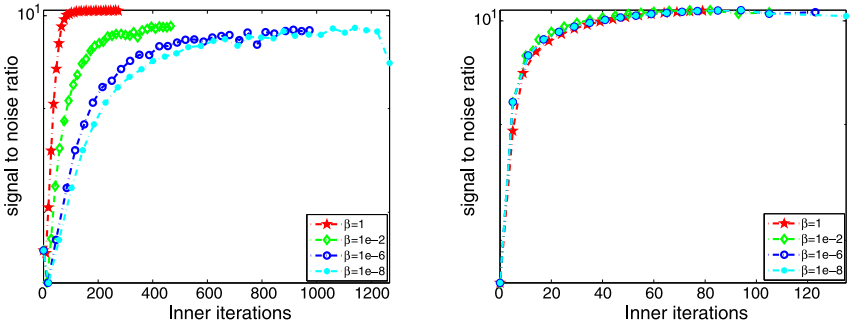

Fig. 4. The descriptions for the change of SNR with different β by fixed point curvature method (left) and homotopy method (right).

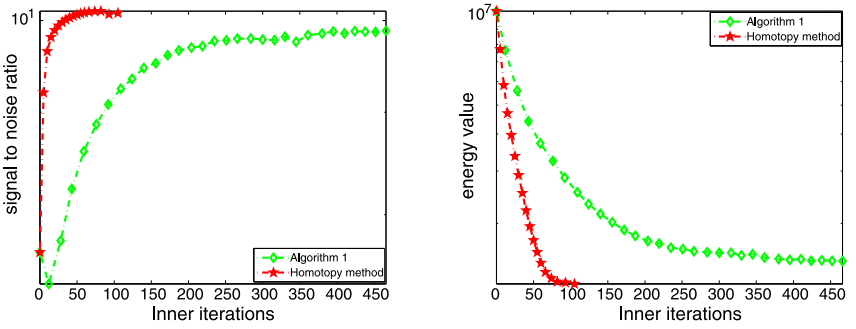

Fig. 5. The comparison of fixed point curvature method with homotopy method for SNR (left) and the energy values (right) with $\alpha = 150$, $\beta = 10^{-4}$.

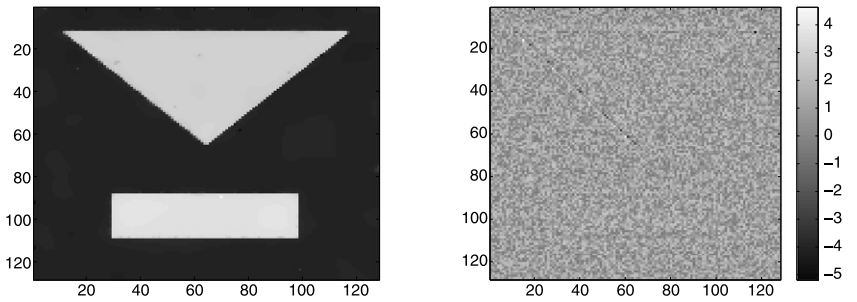

Fig. 6. Image denoised by fixed point curvature method (left) and the difference image (right) with $\alpha = 150$, $\beta = 1$.

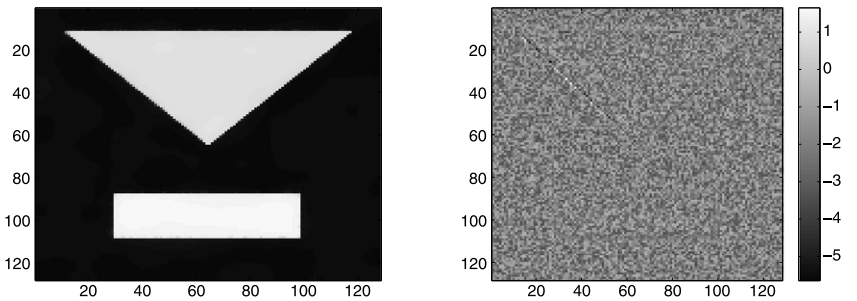

Fig. 7. Image denoised by homotopy method (left) and the difference image (right) with $\alpha = 150$, $\beta = 1$.

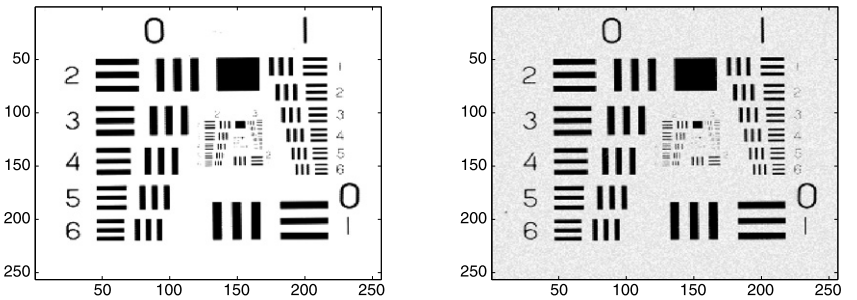

Fig. 8. Original "chart" image (left) and noisy image (right).

5.2. Comparisons of the TV model and surface fitting method with homotopy method for mean curvature model

The classical TV model is known to yield satisfactory results for removing noise while preserving edges and contours of nonsmooth objects. Surface fitting method for a high order model proposed by Lysaker, Osher and Tai [30] improves the quality of restoration by enhancing the recovery of smooth subsurfaces contained in the image. In this section, we conduct numerical experiments to compare these methods with our homotopy method for a mean curvature-based model.

Example 1. It is known that the TV model yields piecewise constant images, so it works well for "blocky" images. A block image with zero mean Gaussian random noise is taken in our first test; the original image and the noisy image are shown in Fig. 8. From the restored results of Figs. 9–11, we see that the recovered image by the TV model preserves the edges well and has a clearer background than the other two methods, and images recovered by surface fitting method and homotopy curvature method are also visually acceptable. In case of the difference images, it is remarkable that mainly the maximum of the difference decreases, comparing the surface fitting method or the homotopy method with classical TV model, while the minimum stays constant. This indicates a change in the average intensity of the results (mean of difference image not zero). On the other side, a decrease in structure can be observed in these figures.

Example 2. Our next example uses the "Barbara" image, see Fig. 12. The challenge with this image is to maintain both texture details and smooth transitions in the face during restoration. From the restored results of Figs. 13–15, we see that the restored images by the surface fitting method and our homotopy curvature method are visually better than the TV model. Similar to Example 1, the difference images indicate some textures on the scarf are oversmoothed by the TV model.

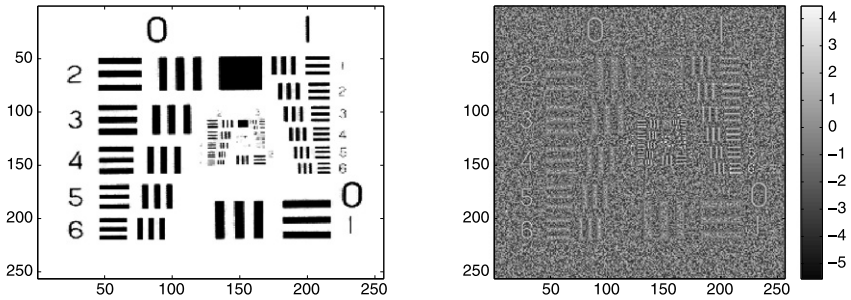

Fig. 9. Image denoised by classical TV model (left) and the difference image (right).

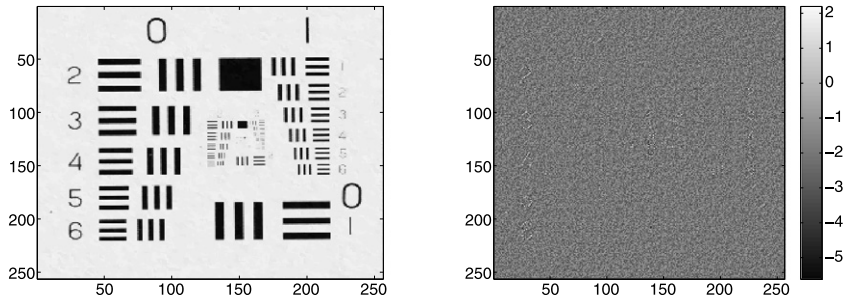

Fig. 10. Image denoised by surface fitting method (left) and the difference image (right).

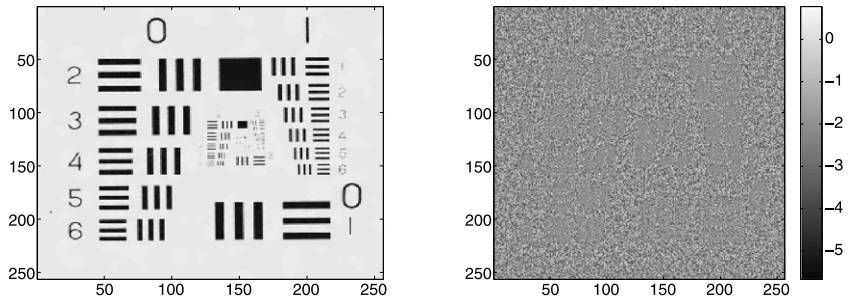

Fig. 11. Image denoised by homotopy method for mean curvature-based model (left) and the difference image (right).

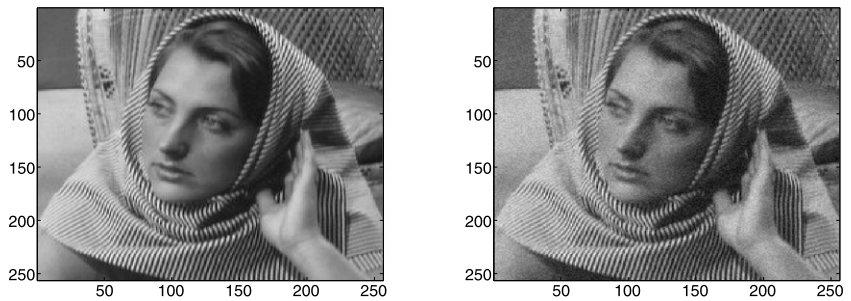

Fig. 12. Original "Barbara" image (left) and noisy image (right).

However, some textures are preserved by surface fitting method and homotopy curvature method. Further, our homotopy curvature method does better than the surface fitting method.

5.3. Comparison of a nonlocal means algorithm with our homotopy method

Test results obtained from comparing the nonlocal means algorithm [8] and our homotopy method for curvature denoising using images of "cameraman" (Fig. 16) and "aircraft" (Fig. 21) with random noise are now shown in Figs. 17–18

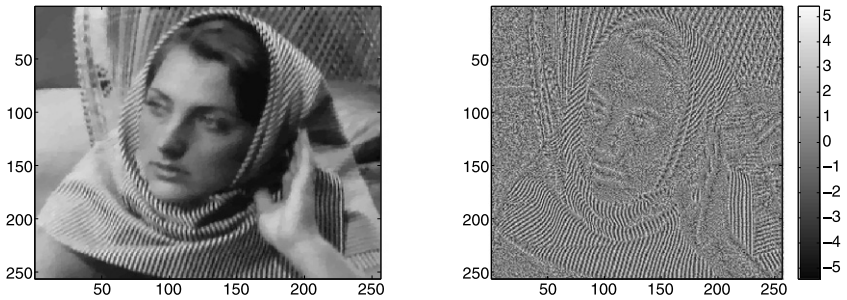

Fig. 13. Image denoised by classical TV model (left) and the difference image (right).

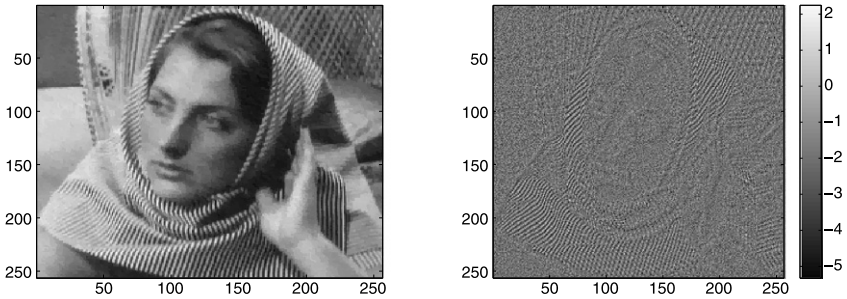

Fig. 14. Image denoised by surface fitting method (left) and the difference image (right).

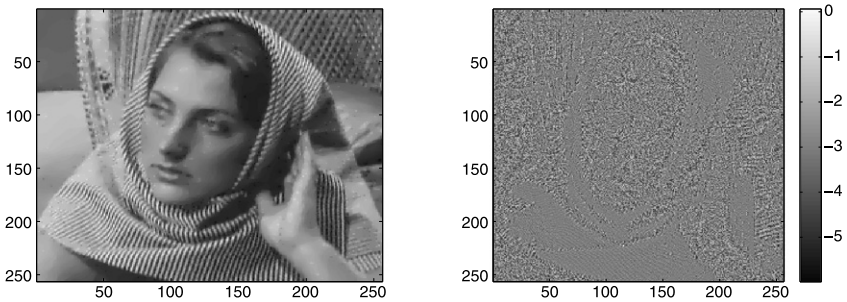

Fig. 15. Image denoised by homotopy method (left) and the difference image (right).

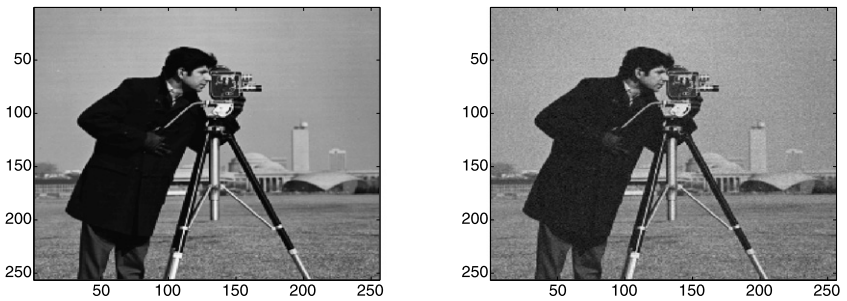

Fig. 16. Original "cameraman" image (left) and noisy image (right).

and 20–21 respectively. In particular, Fig. 22 zooms into a subregion of "aircraft" and Fig. 23 displays the differences of the two methods.

As seen from the recovered images, both methods are able to maintain all important information in the images, and at the same time to filter out noise. As far as the difference images are concerned, one observes that the maximum of the difference for our homotopy curvature method decreases and the nonlocal means algorithm contains less edge structures in the difference image than our homotopy curvature method. However, the nonlocal means algorithm removes more fine details so the maximum of the difference is larger although both recovered subregions (see Fig. 23) provide good visualization. The tests suggest that the mean curvature denoising model is better for contrast preserving and the nonlocal means

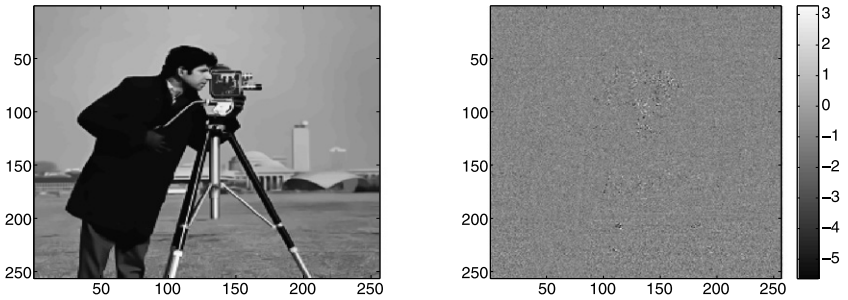

Fig. 17. Image denoised by nonlocal means algorithm (left PSNR = 33.7) and the difference image (right).

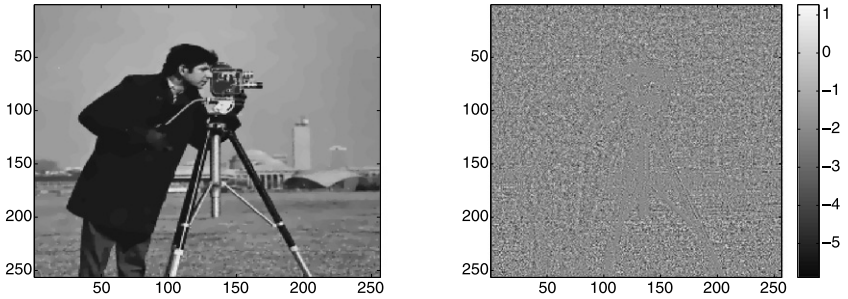

Fig. 18. Image denoised by homotopy method for mean curvature-based model (left PSNR = 33.4) and the difference image (right).

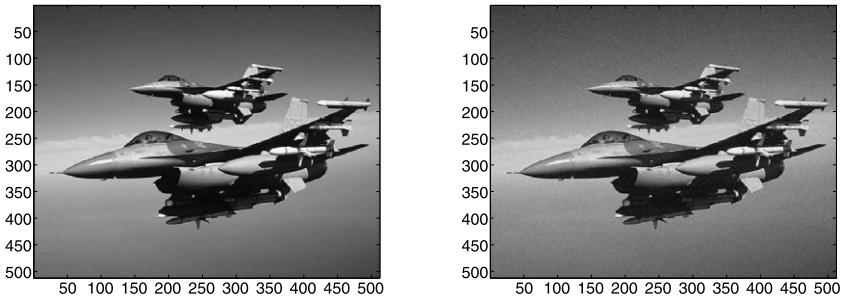

Fig. 19. The original "aircraft" image (left) and noisy image (right PSNR = 23.37).

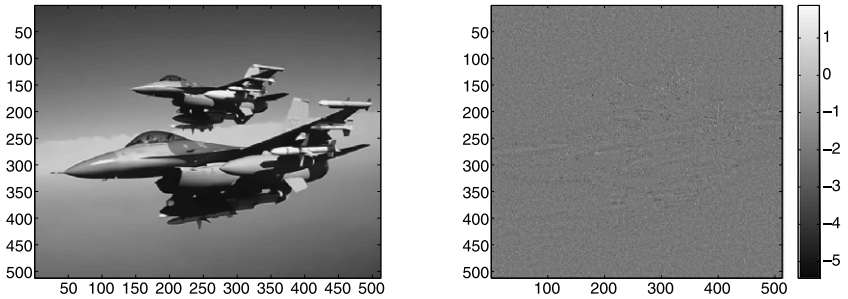

Fig. 20. Images denoised by nonlocal means method (left PSNR = 24.41) and the difference image (right).

algorithm is better for structure preserving, while both are good at reducing staircasing effect of the TV model. In our future work, we hope to compare with the TGV method [5].

6. Conclusions

Curvature-based variational denoising models can restore effectively both blocky images (of piecewise constant intensities) and smooth images (with no clear jumps). For the former case, the restored quality is similar to that from a TV model and for the latter it is much better than the TV. However, the resulting fourth order PDE of a curvature model is much

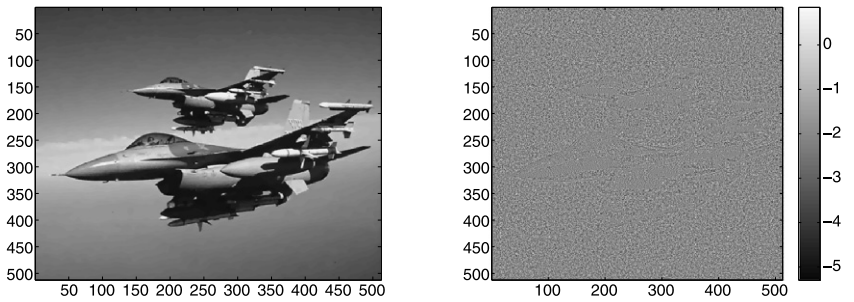

Fig. 21. Images denoised by homotopy method for mean curvature-based model (left PSNR = 24.43) and the difference image (right).

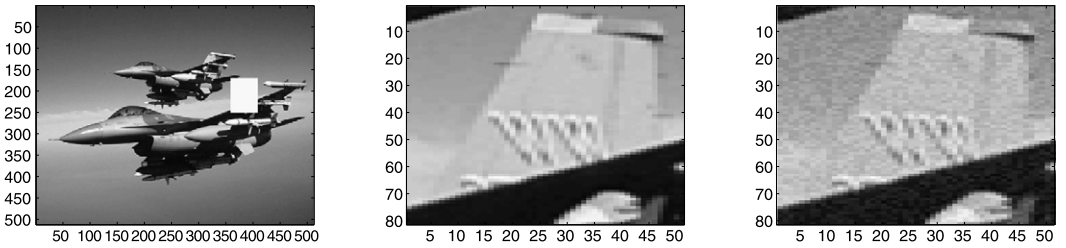

Fig. 22. Marked subregion of "aircraft" image (left), the selected original (middle) and the noisy subregion (right PSNR = 23.37).

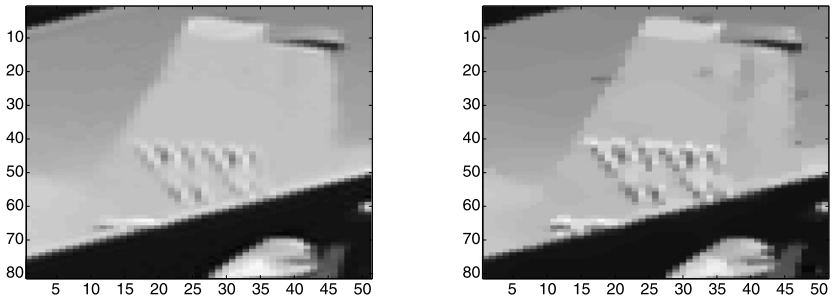

Fig. 23. The subregion denoised by nonlocal means method (left) and homotopy method for mean curvature-based model (right).

more complicated, presenting difficulties for many numerical techniques. Firstly, no simple lagged fixed point methods can be constructed, a working fixed point method from [6] requires stabilization and a relatively large regularization parameter β. Secondly, reformulation methods such as from [44] can provide an elegant solution approach only by solving an approximated problem. This paper first gave a fixed point curvature method for *directly* solving the fourth order PDE and then proposed a homotopy method with curve tracking to choose the regularizing parameter β adaptively. The resulting method turns out to be able to drive the Newton type method (as a corrector) to convergence for a range of test images and for any small parameter β. Numerical experiments can demonstrate advantages of our method over both the TV model and the smoothed normal model. Future work will consider how to make use of our method in a multigrid context as well as for other applications where curvature is used. Of course, it will be of interest to study the solution methods for other effective denoising models [5,28].

References

[1] R. Acar, C.R. Vogel, Analysis of bounded variation penalty methods for ill-posed problems, Inverse Problems 10 (1994) 1217–1229.
[2] E.L. Allgower, K. Georg, Numerical path following, in: Handbook of Numerical Analysis, North-Holland, Amsterdam, 1997.
[3] I.K. Argyros, On the radius of convergence of Newtons method, International Journal of Computer Mathematics 77 (2001) 389–400.
[4] G. Aubert, L.A. Vese, A variational method in image recovery, SIAM Journal of Numerical Analysis 34 (5) (1997) 1948–1979.
[5] K. Bredies, K. Kunisch, T. Pock, Total generalized variation, SIAM Journal on Imaging Sciences 3 (3) (2010) 492–526.
[6] C. Brito-Loeza, K. Chen, Multigrid algorithm for high order denoising, SIAM Journal on Imaging Sciences 3 (3) (2010) 363–389.
[7] C. Brito-Loeza, K. Chen, On high-order denoising models and fast algorithms for vector-valued images, IEEE Transactions on Image Processing 19 (6) (2010) 1518–1527.
[8] A. Buades, B. Coll, J. Morel, A review of image denoising algorithms, with a new one, SIAM Multiscale Modeling and Simulation 4 (2) (2005) 490–530.
[9] E. Catinas, On some iterative methods for solving nonlinear equations, Anal. Numer. Theor. Approx. 23 (1) (1994) 47–53.
[10] A. Chambolle, An algorithm for total variation minimization and applications, Journal of Mathematical Imaging and Vision 20 (2004) 89–97.
[11] A. Chambolle, P.-L. Lions, Image recovery via total variation minimization and related problems, Numerische Mathematik 76 (2) (1997) 167–188.

[12] R.H. Chan, K. Chen, Multilevel algorithm for a Poisson noise removal model with total-variation regularization, International Journal of Computer Mathematics 84 (2007) 1183–1198.
[13] T.F. Chan, G.H. Golub, P. Mulet, A nonlinear primal–dual method for total variation-based image restoration, SIAM Journal on Scientific Computing 20 (6) (1999) 1964–1977.
[14] T.F. Chan, A. Marquina, P. Mulet, High-order total variation-based image restoration, SIAM Journal on Scientific Computing 22 (2000) 503–516.
[15] T.F. Chan, J.H. Shen, Image Processing and Analysis – Variational, PDE, Wavelet, and Stochastic Methods, SIAM, Philadelphia, 2005.
[16] T. Chan, H.M. Zhou, R.H. Chan, Advanced signal processing algorithms, in: F.T. Luk (Ed.), Proceedings of the International Society of Photo-Optical Instrumentation Engineers, SPIE, 1995, pp. 314–325.
[17] Q. Chang, X.-C. Tai, L. Xing, A compound algorithm of denoising using second-order and fourth-order partial differential equations, Numerical Mathematics 2 (4) (2009) 353–376.
[18] S.N. Chow, J. Mallet-Paret, J.A. Yorke, Finding zeros of maps: Homotopy methods that are constructive with probability one, Math. Comput. 32 (1978) 887–899.
[19] J. Dennis, R. Schnabel, Numerical Methods for Unconstrained Optimization and Nonlinear Equations, Prentice-Hall, Englewood Cliffs, NJ, 1983.
[20] C.B. Garcia, W.I. Zangwill, Pathways to Solutions, Fixed Points and Equilibria, Prentice-Hall, Englewood Cliffs, NJ, 1981.
[21] G. Gilboa, S. Osher, Nonlocal operators with applications to image processing, SIAM Multiscale Modeling and Simulation 7 (3) (2008) 1005–1028.
[22] M. Grasmair, F. Lenzen, Anisotropic total variation filtering, Applied Mathematics and Optimization 62 (3) (2010) 323–339.
[23] Y. Huang, M.K. Ng, Y. Wen, A fast total variation minimization method for image restoration, SIAM Multiscale Modeling and Simulation 7 (2) (2008) 774–795.
[24] R.B. Kellogg, T.Y. Li, J.A. Yorke, A constructive proof of the Brouwer fixed-point theorem and computational results, SIAM Journal on Numerical Analysis 18 (1976) 473–483.
[25] S. Kindermann, S. Osher, P. Jones, Deblurring and denoising of images by nonlocal functionals, SIAM Multiscale Modeling and Simulation 4 (4) (2005) 1091–1115.
[26] F. Li, M. Ng, C. Shen, Multiplicative noise removal with spatial-varying regularization parameters, SIAM Journal on Imaging Sciences 3 (2010) 1–20.
[27] Z. Lin, B. Yu, D. Zhu, A continuation method for solving fixed points of self-mappings in general nonconvex sets, Nonlinear Analysis 52 (2003) 905–915.
[28] Y. Lou, X. Zhang, S. Osher, A. Bertozzi, Image recovery via nonlocal operators, Journal of Scientific Computing 42 (2) (2010) 185–197.
[29] M. Lysaker, A. Lundervold, X.-C. Tai, Noise removal using fourth-order partial differential equation with applications to medical magnetic resonance images in space and time, IEEE Transactions on Image Processing 12 (12) (2003) 1579–1590.
[30] M. Lysaker, S. Osher, X.-C. Tai, Noise removal using smoothed normals and surface fitting, IEEE Transactions on Image Processing 13 (10) (2004) 1345–1357.
[31] K. Majava, Optimization-based techniques for image restoration, Ph.D. thesis, University of Jyväskylä, 2001.
[32] A. Marquina, S. Osher, Explicit algorithms for a new time dependent model based on level set motion for nonlinear deblurring and noise removal, SIAM Journal on Scientific Computing 22 (2) (2000) 387–405.
[33] L.A. Melara, A.J. Kearsley, On the Kantorovich Theorem and the regularization parameter in homotopy method for total variation denoising problems, Rocky Mountain J. Math. 40 (2) (2010) 595–607.
[34] L.A. Melara, A.J. Kearsley, R.A. Tapia, Augmented Lagrangian homotopy method for the regularization of total variation denoising problems, Journal of Optimization Theory and Applications 134 (2007) 15–25.
[35] Y.Y. Michael, K. Ng, Liqun Qi, Y. Huang, On semismooth Newton's methods for total variation minimization, Journal of Mathematical Imaging and Vision 27 (3) (2007) 265–276.
[36] S. Osher, M. Burger, D. Goldfarb, J. Xu, W. Yin, An iterative regularization method for total variation-based image restoration, SIAM Multiscale Modeling and Simulation 4 (2) (2005) 460–489.
[37] F.A. Potra, On an iterative algorithm of order 1.839... for solving nonlinear equations, Numerical Functional Analysis and Optimization 7 (1) (1984-85) 75–106.
[38] L.I. Rudin, S. Osher, E. Fatemi, Nonlinear total variation based noise removal algorithms, Physica D 60 (1992) 259–268.
[39] S. Setzer, G. Steidl, T. Teuber, Infimal convolution regularizations with discrete $l1$-type functionals, Communications in Mathematical Sciences 9 (3) (2011) 797–827.
[40] L.A. Vese, A study in the BV space of a denoising-deblurring variational problem, Applied Mathematics and optimization 44 (2) (2001) 131–161.
[41] C.R. Vogel, Computational Methods for Inverse Problems, SIAM, Philadelphia, 2002.
[42] C.R. Vogel, M.E. Oman, Iterative methods for total variation denoising, SIAM Journal on Imaging Sciences 17 (1996) 227–238.
[43] L.T. Watson, C. Billups, P. Morgan, Algorithm 652. HOMPACK: A suite of codes for globally convergent homotopy algorithms, ACM Transactions on Mathematical Software 13 (3) (1987) 281–310.
[44] C. Wu, X.-C. Tai, Augmented Lagrangian method, dual methods, and split Bregman iteration for ROF, vectorial TV, and high order models, SIAM Journal on Imaging Sciences 3 (3) (2010) 300–339.
[45] M.Q. Zhu, Fast numerical algorithms for total variation based image restoration, Ph.D. thesis, UCLA report cam08-44, 2008.
[46] W. Zhu, T. Chan, Image denoising using mean curvature, SIAM Journal on Imaging Sciences (2012), in press.